Alfvén Intermittent Turbulence in Space Plasmas

E. L. Rempel[*], A. C.-L. Chian[*], A. J. Preto[*] and S. Stephany[*]

[*]*National Institute for Space Research (INPE) and World Institute for Space Environment Research (WISER), P.O. Box 515, São José dos Campos–SP, 12227–010, Brazil*

Abstract. We investigate the onset of intermittent chaos in the phase dynamics of nonlinear Alfvén waves in the solar wind by using the Kuramoto-Sivashinsky (KS) equation as a model for phase dynamics. We focus on the role of nonattracting chaotic solutions of the KS equation, known as chaotic saddles, in the transition from weak chaos to strong chaos and show how two of these unstable chaotic saddles can interact to produce the plasma intermittency observed in the strongly chaotic regimes. The dynamical systems approach discussed in this work can lead to a better understanding of the mechanisms responsible for intermittency in solar wind plasmas.

INTRODUCTION

Intermittent fluctuations are constantly encountered in space plasmas, as reported in several works based on the analysis of solar wind data both at the ecliptic [1, 2, 3] and high heliographic latitude [4, 5]. Intermittent events are characterized by time series that display time intervals with low variabilities interrupted by bursts of very high variabilities. As a consequence, the associated probability density functions (PDF's) are non-Gaussian. It has been shown by Vörös et al. [6] and Dorotovic and Vörös [7] that intermittent fluctuations in the solar wind affect the geomagnetic response. By comparing solar wind data obtained from the ACE spacecraft with plasma sheet data from the Geotail mission, Dorotovic and Vörös [7] suggested that the non-Gaussian characteristics of the PDF's of solar wind data can be interconnected to the occurrence of intermittency in the magnetic fluctuations in the plasma sheet. Thus, the study of intermittent phenomena in solar wind plasmas is essential for a better understanding of the solar wind-magnetosphere coupling processes.

The fluctuations of the plasma velocity and magnetic field as revealed by interplanetary data records are frequently well correlated, which is a signature of the presence of Alfvén waves in the solar wind [8, 9]. Alfvén waves are low-frequency electromagnetic waves in a plasma with a background magnetic field. From a linear analysis of MHD equations, the dispersion relation of the Alfvén wave is found as $\omega = k_{\parallel} v_A$, where $k_{\parallel}$ is the component of the wave vector $\mathbf{k}$ parallel to $\mathbf{B}_0$, and $v_A = B_0/(\mu_0 \rho_0)^{1/2}$ is the Alfvén velocity, where B_0 is the strength of the ambient magnetic field, μ_0 is the permeability of vacuum and ρ_0 is the average mass density of the plasma. The perturbation of the fluid velocity $\mathbf{u}$ relates to the magnetic field's perturbation vector $\mathbf{b}=\delta\mathbf{B}_0$ by $\mathbf{u} = \mp\mathbf{b}/(\mu_0 \rho_0)^{1/2}$, where the upper (lower) sign refers to the case $\mathbf{k} \cdot \mathbf{B}_0 > 0$ ($\mathbf{k} \cdot \mathbf{B}_0 < 0$). Thus, $\mathbf{u}$ and $\mathbf{b}$ are parallel/antiparallel and proportional to each other, and the plasma os-

cillates with the magnetic field lines.

As shown by Lefebvre and Hada [10], by assuming weak instability the dynamics of quasiparallel Alfvén waves can be studied by a complex Ginzburg-Landau (CGL) equation. The complex Ginzburg-Landau equation has been one of the most widely studied nonlinear equations in the last decades (see Cross and Hohenberg [11], Bohr et al. [12], Aranson and Kramer [13], and references therein). It describes the slow modulation of a periodic pattern in space and time near the threshold of an instability, where a band of modes become unstable.

In this work we study the phase dynamics of nonlinear Alfvén waves modeled by the CGL equation. Phase dynamics is of particular interest in systems modeled by the CGL equation, since for a range of values of the control parameters the dynamics of perturbations of traveling wave solutions is essentially determined by variations of the phase alone, and can exhibit '*phase turbulence*'. In such regimes the amplitudes are essentially constant and the phase dynamics satisfies the Kuramoto-Sivashinsky (KS) equation [14, 11, 12, 13, 15]. The study of phase dynamics can elucidate important nonlinear phenomena observed in space plasmas. Finite correlation of phases in MHD waves upstream of Earth's bow shock was found in Geotail magnetic field data, indicating that nonlinear interactions between the waves are in progress [16]. This bears important implications in discussions of various transport processes of charged particles in space. In He and Chian [17] imperfect phase synchronization in a nonlinear drift wave system was shown to be responsible for the origin of bursts in wave energy in a turbulent state. Here we focus on the characterization of phase intermittency in the KS equation. We first describe how the fluctuations of the phase can evolve from periodic to chaotic behavior through a sequence of bifurcations as the viscosity is varied. We show that in the KS equation, chaotic attractors coexist with nonattracting chaotic sets responsible for transient chaotic behavior. The collision of a weak chaotic attractor with an unstable periodic orbit leads to the generation of a strong chaotic attractor, in an event known as interior crisis. The post-crisis strong chaotic attractor can be decomposed into two nonattracting chaotic sets, responsible for the generation of intermittent time series.

BASIC CONCEPTS OF NONLINEAR DYNAMICS

In this section we review some basic concepts of nonlinear dynamical systems that are essential for understanding the remaining of this paper.

We consider dissipative dynamical systems described by autonomous systems of ODE's,

$$\dot{\mathbf{x}} = \mathbf{f}(\mathbf{x}), \tag{1}$$

where $\mathbf{x}$ is an n-dimensional vector, $\mathbf{f}$ is a vector function and the dot denotes derivative with respect to time. A *flow* $f_t(\mathbf{x_0})$ is the solution of Eq. (1) for an initial condition $\mathbf{x_0}$ after certain time t. The components of the vector *state variable* $\mathbf{x}$ define a *phase space*, where the flow of $\mathbf{x_0}$ is plotted for increasing values of t, generating the *orbit* of $\mathbf{x_0}$.

A *fixed point* of Eq. (1) is a constant solution, i.e., a point $\bar{\mathbf{x}}$ for which $\dot{\mathbf{x}} = 0$, or equivalently, $f_t(\bar{\mathbf{x}}) = \bar{\mathbf{x}}$ for all t. A *periodic orbit* is a solution of Eq. (1) that always

repeats its behavior after a fixed time interval, i.e., $f_t(\mathbf{x}) = f_{t+T}(\mathbf{x})$ for all t and some minimum period $T > 0$.

Dissipative systems are characterized by the presence of *attractors*. An attractor is a subset of the phase space that attracts almost all the initial conditions in a certain neighborhood, that is, the limit set of the orbits of initial conditions in the neighborhood as time tends to $+\infty$ is the attractor [18]. Attractors may be simple sets like a fixed point or periodic orbit, but can also have nonelementary geometrical properties such as noninteger fractal dimension, in which case the attractor is called *strange* [18, 19]. Fractal sets display scale invariance, which implies that continuous blow-up of a tiny portion of the set reveal self-similar structures on arbitrarily small scales [20].

Strange attractors are typically (but not always) *chaotic* [19]. The orbits of random initial conditions on a chaotic attractor will display aperiodic behavior and *sensitive dependence on initial conditions*, which means that nearby orbits will diverge exponentially with time. The average rate of divergence can be measured by the *Lyapunov exponent*. Let Δ_0 be a small distance separating two initial conditions on the chaotic attractor at $t = 0$. Then for increasing t the orbits of the two points will diverge on average as $\Delta_t \sim \Delta_0 \exp(\lambda t)$, where λ is the Lyapunov exponent [19]. For systems with n-dimensional phase space there are n Lyapunov exponents which measure the rate of divergence/convergence on n orthogonal directions.

Chaotic sets are not necessarily attracting sets. A strange set Λ might be chaotic and nonattracting. That means that the orbits of typical initial conditions in the vicinity of Λ are eventually repelled from it. Nevertheless, Λ contains a chaotic orbit (an aperiodic orbit with at least one positive Lyapunov exponent) [21]. If the chaotic orbit has also one negative Lyapunov exponent the nonattracting chaotic set is known as *chaotic saddle*. Chaotic saddles, as well as chaotic attractors, contain an infinite number of unstable periodic orbits (UPO's).

In nonlinear dynamical systems, as one varies some control parameter present in the model equations some dynamical changes can occur, such as creation/destruction of fixed points and periodic orbits or loss of stability of attracting sets. Thus, periodic attractors can lose their asymptotic stability and become unstable periodic orbits. Similarly, chaotic attractors can lose their attracting nature and become nonattracting chaotic sets, or chaotic saddles. The qualitative changes in the behavior of solutions of dynamical systems as a control parameter is varied are called *bifurcations*. When the changes in the phase portrait involve merely the local vicinity of fixed points or periodic orbits, one has a *local bifurcation*. Large changes in the topology of the system are called *global bifurcations*. An example is the *interior crisis* discussed in this paper, whereby a chaotic attractor is suddenly enlarged. The bifurcations of a dynamical system can be represented in a *bifurcation diagram*, in which the values of one of the state variables are plotted as a function of one control parameter.

A classical technique to analyze nonlinear dynamical systems is the *Poincaré map*. It replaces the flow of an nth-order continuous-time system with an $(n-1)^{th}$-order discrete-time system, simplifying the analysis and visualization of the dynamics. There are different forms of defining a Poincaré map. At the end of the next section we exemplify one of them.

THE KURAMOTO-SIVASHINSKY EQUATION

The derivative nonlinear Schrödinger equation (DNLS) [22, 23] describes the dynamics of quasiparallel Alfvén waves of moderate amplitudes in a finite-β plasma, taking into account weak linear dispersion. To describe patterns formed by Alfvén waves subject to damping and growth rate, Lefebvre and Hada [10] used a model based on a modified version of the DNLS equation, including linear growth rate, linear dissipation and nonlinear Landau damping. Assuming weak instability, Lefebvre and Hada [10] proposed a further simplification to an envelope equation by writing the complex transverse magnetic field $B = B_y + iB_z$ as $B(x,t) = \psi(\xi,t)\exp[i(k_c x - \omega_c t)]$, where $\omega_c = \omega(k_c)$, $\xi = x - v(k_c)t$ and k_c is the most unstable mode. Assuming $k_c > 0$ (left-hand polarization) the resulting equation for ψ is given by

$$\partial_t \psi = \psi + (1 - ib_1)\partial_{\xi\xi}\psi - i\psi(b_2 - H)|\psi|^2, \tag{2}$$

where b_1 measures the strength of the dispersion and b_2 the effects of nonlinearity. The term H denotes a function that accounts for the nonlinear Landau damping [23]. Equation (2) falls into the general class of the complex Ginzburg-Landau equation. The envelope ψ is a complex variable. By writing $\psi = R\exp(i\Phi)$ and assuming small perturbations $R = R_0 + r$, $\Phi = \Phi_0 + \phi$, it is possible to derive an equation for the phase ϕ of the CGL equation. As shown by Kuramoto and Tsuzuki [14] and Aranson and Kramer [13], the phase equation is given by the Kuramoto-Sivashinsky equation. Here we study the following form of the KS equation [24, 25, 26, 27]

$$\partial_t \phi = -\partial_x^2 \phi - \nu\partial_x^4 \phi - \partial_x \phi^2, \tag{3}$$

where ν is a damping parameter representing viscosity and we assume that $\phi(x,t)$ is subject to periodic boundary conditions $\phi(x,t) = \phi(x + 2\pi, t)$.

To obtain the numerical solution of Eq. (3) we use the spectral Galerkin method, by applying a Fourier decomposition for the function $u(x,t)$, $u(x,t) = \sum_{k=-\infty}^{\infty} b_k(t)e^{ikx}$, which yields an infinite set of ordinary differential equations for the complex Fourier coefficients $b_k(t)$. To simplify the analysis we restrict our attention to the subspace of odd functions $u(x,t) = -u(-x,t)$ and assume $b_k(t)$ purely imaginary by setting $b_k(t) = -ia_k(t)/2$, where $a_k(t)$ are real. The final set of equations is given by [25, 26, 27]

$$\dot{a}_k(t) = (k^2 - \nu k^4)a_k(t) - \frac{k}{2}\sum_{m=-N}^{N} a_m(t)a_{k-m}(t), \tag{4}$$

where the dot denotes derivative with respect to t, and $1 \le k \le N$, N is the truncation order.

The choice of the truncation N for the number of modes has obvious implications in the numerical solutions of Eq. (3). For this work we choose a set of control parameter values in which the energy is concentrated in the low-k long wavelength modes. A spatiotemporal pattern $\phi(x,t)$, obtained using $N = 16$ modes and $\nu = 0.029919$, is shown in Fig. 1. The system dynamics is chaotic in time but coherent in space.

The dynamics of the system described by Eq. (4) can be analyzed on a Poincaré section defined by $a_1 = 0$. We adopt a Poincaré map P defined as the $(N-1)$ dimensional
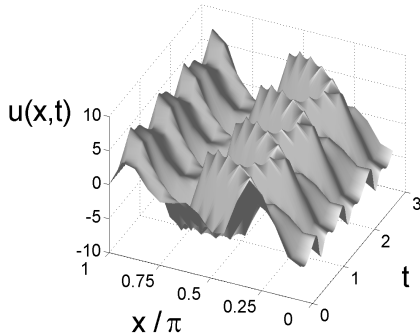
FIGURE 1. Spatiotemporal pattern of $\phi(x,t)$ for $v = 0.029919$. The system dynamics is chaotic in time but coherent in space.

hyperplane given by $a_1 = 0$, with $\dot{a}_1 > 0$, so that a Poincaré point is plotted every time the flow of Eq. (4) crosses the Hyperplane $a_1 = 0$ from "left" to "right".

NONLINEAR DYNAMICS ANALYSIS

The bifurcation diagram

Figure 2(a) depicts the bifurcation diagram $a_6(v)$ for Eq. (4) with $N = 16$. The diagram is similar for any choice of a_k. For this range of v, the attracting set can be either chaotic or periodic. The gray area in Fig. 2(a) depicts another important subset of the phase space representing a chaotic saddle. The trajectories of random initial conditions are first attracted to the vicinity of the chaotic saddle, where they display chaotic behavior for a finite time (*chaotic transient*), before they converge to the attractor (periodic or chaotic). The chaotic saddles are obtained by the PIM triple algorithm [21]. In Fig. 3 an example of transient chaos is shown for a time series of Poincaré points at $v = 0.0299248$, where the phase dynamics converges to a p-3 attractor.

A saddle-node bifurcation at $v = v_{SNB} \approx 0.02992498$, indicated as SNB in Fig. 2, marks the beginning of a *periodic window* in the bifurcation diagram. For $v > v_{SNB}$, random initial conditions converge to a chaotic attractor, and for $v < v_{SNB}$ the chaotic attractor no longer exists. At the saddle-node bifurcation the simultaneous creation of a p-3 attractor and a p-3 unstable periodic orbit occurs. The p-3 UPO, found with the Newton method, is represented in Fig. 2(a) by dashed lines. As the value of v is decreased, the p-3 attractor undergoes a cascade of period-doubling bifurcations, whereby the period of the attractor is successively doubled. As the period tends towards infinity, a chaotic attractor is formed, localized in three separate bands in the bifurcation diagram. We call the region occupied by this "banded" attractor the *band region* (B), and the region occupied by the surrounding chaotic saddle (SCS) the *surrounding region* (S), following reference [28]. At $v = v_{IC} \approx 0.02992021$ the chaotic attractor collides with the p-3 UPO created at SNB, called the *mediating unstable periodic orbit* (MPO). This
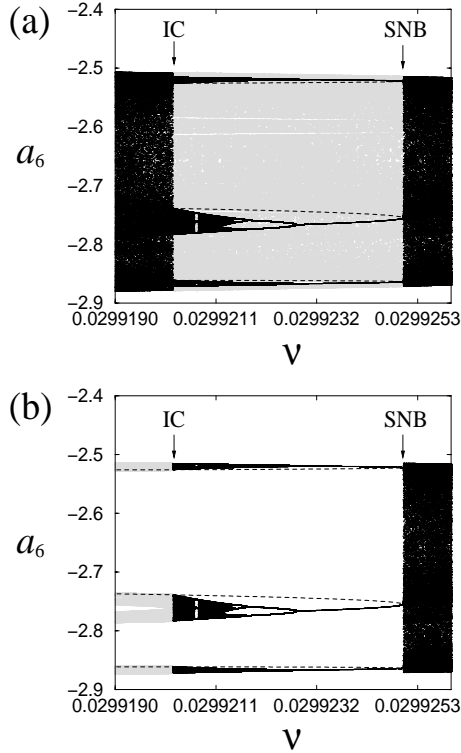
FIGURE 2. (a) Variation of a_6 for the chaotic saddle (gray) as a function of ν, superimposed by the bifurcation diagram of the attractor (black) in a p-3 periodic window. IC denotes interior crisis and SNB denotes saddle-node bifurcation. The dashed lines denote the p-3 mediating unstable periodic orbit. (b) Same as (a), but depicting the conversion of the three-band weak chaotic attractor into a band chaotic saddle after (to the left of) IC.

collision is responsible for an *interior crisis*, which is a sudden enlargement in the size of a chaotic attractor [29]. The value of the maximum Lyapunov exponent (λ_{max}) jumps abruptly from $\lambda_{max} \approx 0.3$ just before crisis to $\lambda_{max} \approx 0.6$ right after crisis, indicating a sudden increase in the attractor's chaoticity. For that reason, the pre-IC chaotic attractor is called *weak chaotic attractor* and the post-IC attractor, the *strong chaotic attractor*. Figure 4 shows a three-dimensional projection (a_1, a_{10}, a_{16}) of the Poincaré points of the strong chaotic attractor (SCA, light line) after crisis $(\nu = 0.02992006)$, superimposed by the 3-band weak chaotic attractor (WCA, dark lines) at crisis $(\nu = 0.02992021)$.

After crisis $(\nu < \nu_{IC})$, we find a new chaotic saddle embedded in the enlarged chaotic attractor, in the region previously occupied by the "pre-IC" banded chaotic attractor. In contrast with the surrounding chaotic saddle, we call this new chaotic saddle the *band chaotic saddle* (BCS). Figure 2(b) illustrates the structure of BCS after IC, where the bifurcation diagram for the attractor (black) of Fig. 2(a) is plotted to the right of the IC point and the band chaotic saddle (gray) is plotted to the left of IC. It is important to stress that although in Fig. 2(a) the surrounding chaotic saddle is plotted only between
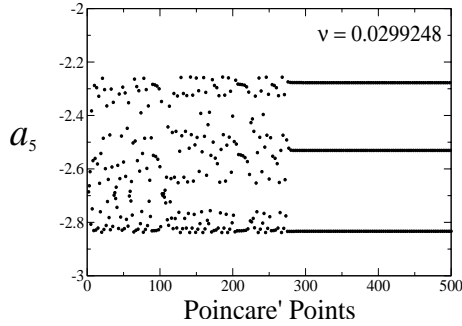
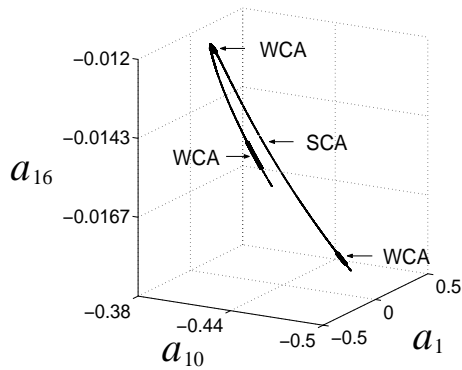**FIGURE 3.** Transient chaos at $\nu = 0.0299248$.

FIGURE 4. Three-dimensional projection (a_1, a_{10}, a_{16}) of the strong chaotic attractor (SCA, light line) defined in the 15-dimensional Poincaré hyperplane after crisis at $\nu = 0.02992006$, superimposed by the three-band weak chaotic attractor (WCA, dark lines) at crisis $(\nu = 0.02992021)$.

points SNB and IC, it is actually present in the entire bifurcation diagram. For $\nu < \nu_{IC}$ and $\nu > \nu_{SNB}$ SCS is a subset of the chaotic attractor.

Crisis-induced intermittency

After the crisis, it is still possible to determine the B and S regions, which are separated by the stable manifold of MPO. Since MPO is a saddle point of the Poincaré map it has associated stable and unstable manifolds. The stable manifold is the set of points that converge to MPO in forward time dynamics; the unstable manifold is the set of points that converge to MPO in the time reversed dynamics. Figure 5 shows a 2-D $(a_5$ vs. $a_6)$ projection of the chaotic sets for $\nu = 0.02992006$, after the crisis, around the upper branch of the strong chaotic attractor shown in Fig. 4. Figure 5(a) shows the chaotic attractor (CA) and Fig. 5(b) shows the corresponding B (light lines) and S (dark lines) chaotic saddles. BCS is localized in a region of the phase space previously
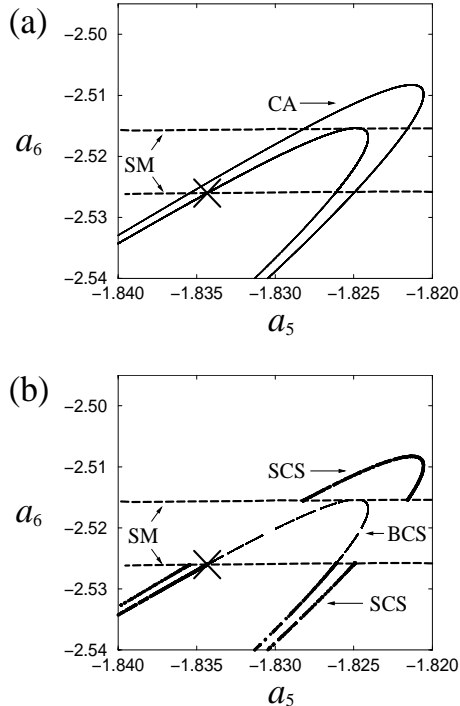
FIGURE 5. (a) Upper branch of the chaotic attractor (CA) after the interior crisis, at $\nu = 0.02992006$. The dashed lines indicate segments of the stable manifolds (SM) of the mediating unstable periodic orbit (cross); (b) the band chaotic saddle (BCS, light lines) and the surrounding chaotic saddle (SCS, dark lines) that compose the chaotic attractor shown in (a).

occupied by the pre-crisis weak chaotic attractor. SCS is the continuation of the pre-crisis surrounding chaotic saddle. It can be seen from Fig. 5 that the post-crisis B and S chaotic saddles are subsets of the strong chaotic attractor. Unlike the chaotic attractor, the chaotic saddles appear as discontinuous lines in the Poincaré map. They have many gaps, most of which are not visible in Fig. 5 due to their small size. The gaps in SCS and BCS are filled by a set of coupling UPO's created at the crisis [30].

The two post-IC chaotic saddles are not attracting, but they exert influence on the dynamics of nearby orbits, since they are responsible for chaotic transients. For $\nu > \nu_{IC}$, trajectories on the chaotic attractor never abandon the band region. For ν slightly less than ν_{IC} a trajectory started in the B region can stay in B for a long time, after which it crosses SM and escapes to region S. Once it is in the surrounding region, the trajectory is in the neighborhood of SCS. Since SCS is nonattracting, after some time the trajectory is "re-injected" into region B. The "jumps" between regions B and S repeat intermittently. This crisis-induced intermittency can be viewed as an alternation between two transient behaviors, in which the trajectory spends a finite time in the vicinity of either BCS or SCS. These transitions between regions B and S are due to the coupling UPO's that are located within the gaps of BCS and SCS, and establish the dynamical
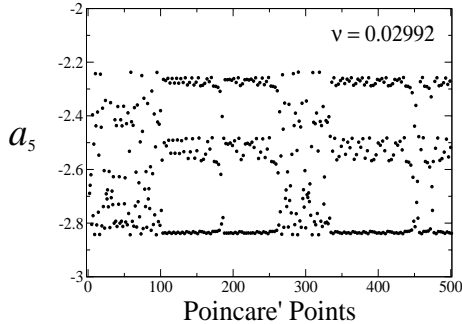
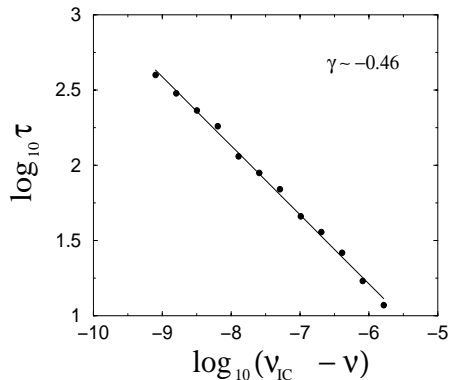**FIGURE 6.** Crisis-induced intermittency at $\nu = 0.02992$.

FIGURE 7. $\log_{10}\tau$ vs $\log_{10}(\nu_{IC} - \nu)$. The solid line with slope $\gamma \approx -0.46$ is a linear fit of the values of the characteristic intermittency time τ computed from time series (circles).

connection between the two chaotic saddles [28, 31]. The crisis-induced intermittency is characterized by time series containing weakly chaotic laminar phases that are randomly interrupted by strongly chaotic bursts, as shown in Fig. 6 for $\nu = 0.02992$. The weakly chaotic laminar phases correspond to the time spent in region B, and the strongly chaotic bursts correspond to the time spent in region S.

The average duration of the "laminar" phases in the intermittent time series (the *characteristic intermittency time*) depends on the value of ν. Close to ν_{IC} the average time spent in the vicinity of BCS is very long, and decreases as ν is decreased away from ν_{IC}. The characteristic intermittency time (denoted by τ) can be obtained as the average over a long time series of the time between switches among regions B and S. Figure 7 is a plot of $\log_{10}\tau$ vs $\log_{10}(\nu_{IC} - \nu)$, where the solid line with slope $\gamma \approx -0.46$ is a linear fit of the values of the characteristic intermittency time computed from time series (circles). Figure 7 reveals that the characteristic time τ decreases with the distance from the critical parameter value ν_{IC} following a power-law decay, $\tau \sim (\nu_{IC} - \nu)^{\gamma}$, as expected [32].

CONCLUSIONS

We have investigated the relevance of chaotic saddles and unstable periodic orbits at the onset of intermittent chaos in the phase dynamics of nonlinear Alfvén waves by using the Kuramoto-Sivashinsky equation as a model equation. We described how a strong chaotic attractor formed after an interior crisis can be naturally decomposed into two nonattracting chaotic sets, known as chaotic saddles, dynamically linked by a set of coupling unstable periodic orbits. The perturbed wave phase oscillates irregularly, switching intermittently from the neighborhood of one nonattracting chaotic set to the other.

The dynamical scenario described in this paper reflects a situation of intermittency in chaotic spatiotemporal systems that is still distant from the well-developed turbulent regimes found in space plasmas, where one expects a huge number of modes to become actively involved in the dynamics. Nevertheless, we believe the dynamical systems approach discussed in this work may be helpful to understand more complex cases. Several authors have searched for evidence of deterministic chaos in space plasmas. Pavlos et al. [33] found evidence of a low-dimensional chaotic attractor in the solar wind through the determination of the correlation dimension from time series of the magnetic field obtained by the IMP-8 spacecraft at 1 AU. A low value for the correlation dimension obtained from solar wind data was also reported in other works [2, 34]. Macek and Obojska [35], Macek and Redaelli [36] and Redaelli and Macek [37] estimated the Lyapunov exponents, fractal dimension and the Kolmogorov entropy from solar wind data obtained by the Helios 1 spacecraft in the inner heliosphere, concluding that the solar wind is likely a deterministic chaotic system. Sorriso-Valvo et al. [38] studied plasma intermittency by using a simplified shell model which mimics 3-D MHD equations. They showed that, just like in solar wind data, the intermittency displayed by the shell model is characterized by a strong departure from Gaussian behavior in the probability density functions for the velocity and magnetic field fluctuations at small scales. Although it is not possible to state that the erratic fluctuations observed in the real world are simple manifestations of chaos, in the works mentioned above the behavior observed in nature seems to have a strong deterministic component. Thus, the study of dynamical systems can lead to a better understanding of the mechanisms responsible for the onset of intermittent turbulence in space plasmas. In fact, space data are a mixture of both stationary and nonstationary components. Therefore we can perform space data analysis using either deterministic or statistical techniques. Most works on solar wind intermittency are based on statistical analysis [1, 2, 6, 3, 7]. Our theoretical study of solar wind intermittency based on chaos theory provides new insights to extend the deterministic analysis of solar wind data [35, 36, 37] to deepen our understanding of solar wind intermittency. In particular, our theoretical results can be used to reconstruct chaotic transients in phase space from space data and to calculate the average duration of laminar phases in solar wind intermittency.

ACKNOWLEDGMENTS

REFERENCES

1. L. F. Burlaga, *J. Geophys. Res.*, **96**, 5847–5851 (1991).
2. E. Marsch, and C.-Y. Tu, *Ann. Geophys.*, **11**, 227–238 (1993).
3. R. Bruno, V. Carbone, L. Sorriso-Valvo, and B. Bavassano, *J. Geophys. Res.*, **108**, 1130–1145 (2003).
4. A. A. Ruzmaikin, J. Feynman, B. E. Goldstein, E. J. Smith, and A. Balogh, *J. Geophys. Res.*, **100**, 3395–3404 (1995).
5. C. Pagel, and A. Balogh, *J. Geophys. Res.*, **108**, 1012–1028 (2003).
6. Z. Vörös, D. Jankovicová, and P. Kovács, *Nonlin. Proc. Geophys.*, **9**, 149–162 (2002).
7. I. Dorotovic, and Z. Vörös, *Proceedings IAU Symposium*, **223**, in press (2004).
8. J. W. Belcher, and L. Davis, *J. Geophys. Res.*, **76**, 3534–3563 (1971).
9. M. L. Goldstein, and D. A. Roberts, *Ann. Rev. Astron. Astrophys.*, **33**, 283–325 (1995).
10. B. Lefebvre, and T. Hada, *Eos Transactions of AGU, Fall Meeting Supplement*, **81**, Abstract SM62A–09 (2000).
11. M. C. Cross, and P. C. Hohenberg, *Rev. Mod. Phys.*, **65**, 851–1112 (1993).
12. T. Bohr, M. H. Jensen, G. Paladin, and A. Vulpiani, *Dynamical systems approach to turbulence*, Cambridge University Press, Cambridge, 1998.
13. I. S. Aranson, and L. Kramer, *Rev. Mod. Phys.*, **74**, 99–143 (2002).
14. Y. Kuramoto, and T. Tsuzuki, *Prog. Theor. Phys.*, **55**, 356–369 (1976).
15. G. van Baalen, *Commun. Math. Phys.*, **247**, 613–654 (2004).
16. T. Hada, D. Koga, and E. Yamamoto, *Spa. Sci. Rev.*, **107**, 463–466 (2003).
17. K. F. He, and A. C.-L. Chian, *Phys. Rev. Lett.*, **3**, 034102 (2003).
18. C. Grebogi, E. Ott, S. Pelikan, and J. A. Yorke, *Physica D*, **13**, 261–268 (1984).
19. C. Grebogi, E. Ott, and J. A. Yorke, *Science*, **238**, 585–718 (1987).
20. E. Ott, *Chaos in dynamical systems*, Cambridge Univ. Press, Cambridge, 1993.
21. H. E. Nusse, and J. A. Yorke, *Physica D*, **36**, 137–156 (1989).
22. A. Rogister, *Phys. Fluids.*, **14**, 2733 (1971).
23. E. Mjolhus, and J. Wyller, *J. Plasma Phys.*, **40**, 299–318 (1988).
24. R. E. LaQuey, S. M. Mahajan, P. H. Rutherford, and W. M. Tang, *Phys. Rev. Lett.*, **34**, 391–394 (1975).
25. F. Christiansen, P. Cvitanović, and V. Putkaradze, *Nonlinearity*, **10**, 55–70 (1997).
26. A. C.-L. Chian, E. L. Rempel, E. E. Macau, R. R. Rosa, and F. Christiansen, *Phys. Rev. E*, **65**, 035203(R) (2002).
27. E. L. Rempel, and A. C.-L. Chian, *Phys. Lett. A*, **319**, 104–109 (2003).
28. K. G. Szabó, Y.-C. Lai, T. Tél, and C. Grebogi, *Phys. Rev. E*, **61**, 5019–5032 (2000).
29. C. Grebogi, E. Ott, and J. A. Yorke, *Physica D*, **7**, 181–200 (1983).
30. C. Robert, K. T. Alligood, E. Ott, and J. A. Yorke, *Physica D*, **144**, 44–61 (2000).
31. E. L. Rempel, and A. C.-L. Chian, *Int. J. Bifurcation Chaos*, **14**, in press (2004).
32. C. Grebogi, E. Ott, F. Romeiras, and J. A. Yorke, *Phys. Rev. A*, **36**, 5365–5380 (1987).
33. G. P. Pavlos, G. A. Kyriakou, A. G. Rigas, P. I. Liatsis, P. C. Trochoutsos, and A. A. Tsonis, *Ann. Geophys.*, **10**, 309–322 (1992).
34. L. F. Burlaga, *Interplanetary Magnetohydrodynamics*, Oxford University Press, Oxford, 1995.
35. W. M. Macek, and L. Obojska, *Chaos Solitons Fractals*, **8**, 1601–1607 (1997).
36. W. M. Macek, and S. Redaelli, *Phys. Rev. E*, **62**, 6496–6504 (2000).
37. S. Redaelli, and W. M. Macek, *Planet. Space Sci.*, **49**, 1211–1218 (2001).
38. L. Sorriso-Valvo, V. Carboni, P. Giulinani, P. Veltri, R. Bruno, V. Antoni, and E. Martines, *Planet. Space Sci.*, **49**, 1193–1200 (2001).